Available online at www.sciencedirect.com
SCIENCE DIRECT®
Journal of Sound and Vibration 288 (2005) 345–360
JOURNAL OF SOUND AND VIBRATION
www.elsevier.com/locate/jsvi

Development of hybrid method for the prediction of underwater propeller noise

Hanshin Seol[a], Jung-Chun Suh[b,*], Soogab Lee[c,*]

[a]*Korea Research Institute of Ships and Ocean Engineering (KRISO), KORDI, Jang-Dong 171, P.O. Box 23, Yusung-Gu, Daejeon 305-343, Republic of Korea*
[b]*Department of Naval Architecture and Ocean Engineering, BD 42, Seoul National University, Seoul 151-742, Republic of Korea*
[c]*School of Mechanical and Aerospace Engineering, Seoul National University, Shinlim-Dong, Kwanak-Ku, BD 311-105, Seoul 151-742, Republic of Korea*

Received 15 March 2004; received in revised form 4 January 2005; accepted 13 January 2005
Available online 25 March 2005

Abstract

Noise reduction and control is an important problem in the performance of underwater acoustic systems and in the habitability of the passenger ship for crew and passenger. Furthermore, sound generated by a propeller is critical in underwater detection and it is often related to the survivability of the vessel especially for military purpose. This paper presents a numerical study on the non-cavitating and blade sheet cavitation noises of the underwater propeller. A brief summary of numerical method with verification and results are presented. The noise is predicted using time-domain acoustic analogy. The flow field is analyzed with potential-based panel method, and then the time-dependent pressure and sheet cavity volume data are used as the input for Ffowcs Williams–Hawkings formulation to predict the far-field acoustics. Noise characteristics are presented according to noise sources and conditions. Through this study, the dominant noise source of the underwater propeller is analyzed, which will provide a basis for proper noise control strategies.

*Corresponding author. Institute of Advanced Aerospace Technology, School of Mechanical and Aerospace Engineering, Seoul National University, Shinrim-Dong, Kwankal-Ku, BD 311-105, Seoul 151-742, Korea. Tel.: 822 02 880 7384; fax: 822 02 887 2662.
E-mail addresses: hsseol@kriso.re.kr (H. Seol), solee@plaza.snu.ac.kr (S. Lee).

0022-460X/$ - see front matter © 2005 Elsevier Ltd. All rights reserved.
doi:10.1016/j.jsv.2005.01.015

Nomenclature

c_0	speed of sound
$f(\vec{x},t)=0$	equation of blade surface
l_i	local force per unit area on fluid in direction i
M	Mach number
M_r	Mach number in radiation direction
$\hat{n}$	unit outward normal vector to surface $f=0$
$p'(\vec{x},t)$	acoustic pressure
r	length of radiation vector, $\lvert\vec{x}-\vec{y}\rvert$
$\vec{r}$	radiation vector, $\vec{x}-\vec{y}$
$\hat{r}$	unit radiation vector, $\vec{r}/r$
t	observer time
$\hat{t}$	unit tangent vector to surface $f=0$
v_n	local normal velocity of blade surface
$\vec{v}$	local velocity of blade surface
$\vec{x}$	observer position in frame
$\vec{x}_{\mathrm{OBS}}$	observer location
$\vec{y}$	source position
$\vec{y}_0(t)$	position vector from origin of ground-fixed frame to moving frame
τ	source time
ret	evaluated at retarded or emission time

1. Introduction

Sound generated by a propeller is critical in underwater detection, and it is often related to the survivability of the vessels especially for military purposes. The propeller generally operates in a non-uniform wake field behind the vessel. As the propeller rotates, it is subjected to unsteady force, which leads to discrete tonal noise, and cavitation. Therefore, underwater propeller noise can be classified into cavitating and non-cavitating noise. Cavitation of the underwater propeller is the most prevalent source of underwater sound in the ocean and it is often the dominant noise source of a marine vehicle. In the past, the propeller design philosophy has been avoiding cavitation for the widest possible range of operating conditions. However, the recent demands for high vehicle speed and high propeller load have made this designing philosophy practically impossible to achieve. Therefore, underwater propeller cavitation has been more and more common in recent ocean vehicle application. In the mean time, submarines and torpedoes are usually operated under the deep sea enough to avoid cavitation [1]. So both cavitating and non-cavitating noise are also important. The approach for the investigation of the underwater propeller noise is a potential-based panel method coupled with acoustic analogy. Among the various types of cavitation noise, unsteady sheet cavitation on the suction surface is known to produce the highest noise level [1].

Sheet cavitation noise results from the growth and collapse of a sheet of bubbles occupying a volume on the individual blades. Fig. 1 shows the general noise spectrum of a cavitating propeller [2]. Sheet cavitation radiates sound from 5 Hz to more than 10 kHz. Low frequency noise (region I and II) is caused by the fluctuations of the sheet cavitation volumes possibly represented by a large bubble that acts as an acoustic monopole. On the other hand, high-frequency noise (region III and IV) is caused by sheet cavity collapse or by shock wave generation [2]. For many years, the sheet cavity has been considered as a single valued volume of vapor attached to the surface, which can be calculated by potential flow methods [3]. In the present study, computational method for the analysis of the propeller noise in non-uniform inflow is newly developed. Flow results, the time-dependent cavity volume and blade surface pressure data, are used as the input for blade sheet cavitation noise analysis in the blade rate frequency and its harmonics (low-frequency region). But

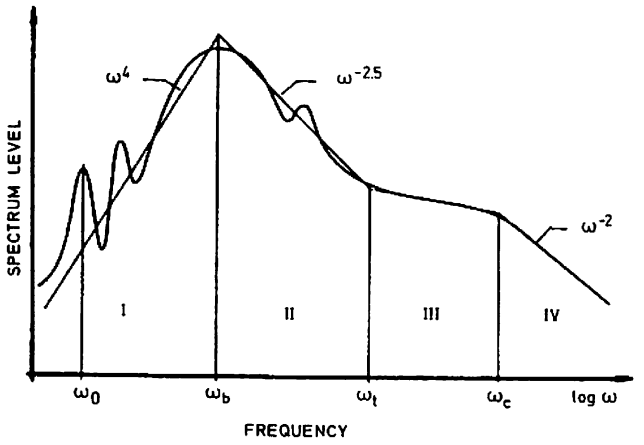

Fig. 1. General noise spectrum of a cavitating propeller (from Ref. [2]).

high-frequency noise analysis is excluded in this study because it is too complex to model the real cavity collapse and shock wave dominated by nonlinearity. In the field of propeller cavitation study, presently numerical technology is still too poor to describe that kind of nonlinearity and complexity. In addition, the sound pressure level of the high-frequency noise is much lower than that of the low frequency noise [2].

A brief description of the flow analysis methodology is given along with verification. The panel method developed in this study is an embodiment of the classical Green's third identity for velocity potential with Kutta condition to ensure uniqueness. The flow solver employs hyperboloidal panel elements on the exact surfaces of the propeller blades, containing all the complications of skew, rake and pitch changes found in most marine propellers. With improved Kutta condition, this method is proved to be robust and accurate.

For a given cavitation number, the cavity shape is determined by satisfying both the kinematic and the dynamic boundary condition on the cavity boundary under cavitation condition. This method is then extended to include the effect of the supercavitation and the analysis of time-varying cavitating flows around the propeller blades. To reduce the computing time, a split panel method is applied [4].

Noise prediction is performed using time-domain acoustic analogy. There are various ways to evaluate Ffowcs Williams–Hawkings equation and the three types of noise source terms (monopole, dipole, and quadrupole) proposed [5]. Farassat proposed a time-domain formulation that can predict noise from an arbitrary shaped object in motion without the numerical differentiation of the observer time [6,7]. The implementation of this formulation is quite straightforward because contributions from each panel with different retarded times are added to form an acoustic wave. The quadrupole noise source term is neglected in this study since the rotating speed of the propeller is much lower than the speed of sound in water.

Through these studies, the dominant noise source of underwater propeller is analyzed, which will provide a basis for proper noise control strategies.

2. Methodology

2.1. Flow solver

There are many kinds of panel methods to solve aerodynamic and hydrodynamic applications. Hess [8] proposed the surface source method and Morino [9] first introduced the Kutta condition for the potential-based panel method. Panel methods and their application to propeller technology began in the 1980s. A potential-based panel method for marine propeller was developed by Kerwin and Lee [10] at MIT in 1978 and Hsin developed a panel method for solving marine propellers in unsteady flow. The fundamentals and details of panel method are well described in works of Hsin [11], Kerwin et al. [12], Pyo et al. [13], and Kinnas and Fine [14], therefore, only a brief description is given here. The method is based on Green's third identity for velocity potential ϕ.

$$2\pi\phi = \int_S \left[\phi \frac{\partial G}{\partial n} - G\frac{\partial \phi}{\partial n}\right] \mathrm{d}S + \int_{S_W} \Delta\phi \frac{\partial G}{\partial n} \mathrm{d}S. \tag{1}$$

Here, the body surface S is composed of propeller blade surface S_B and hub surface S_H. The wake surface S_W is the propeller wake surface. The surfaces and wakes of propeller are discretized into hyperboloidal panels, where dipoles and sources of constant strength are distributed. The Kutta condition [13] is used and the pressure equality at the trailing edge of the blade is also enforced. Eq. (1) yields a unique solution using the Kutta condition. The panel method for solving the unsteady propeller problem was developed by Hsin [11]. This method is based on a discrete time-stepping algorithm. Integral equation (1) is solved at each time step and the time-dependent terms of Eq. (1) are updated for the next time step. The discretized form of Eq. (1) is as follows:

$$\sum_{j=1}^{N_P} a_{i,j}\phi_j(n) + \sum_{m=1}^{M_B} W_{i,m,1}\Delta\phi_{m,1}(n) = \mathrm{RHS}_i(n), \quad i = 1, 2, \ldots, N_P, \tag{2}$$

$$\begin{aligned}\mathrm{RHS}_i(n) = &\sum_{K=1}^{N_B}\sum_{j=1}^{N_P} b_{i,j}^K \sigma_j^K(n) - \sum_{K=2}^{N_B}\sum_{j=1}^{N_P} a_{i,j}^K \phi_j^K(n) \\ &- \sum_{K=2}^{N_B}\sum_{m=1}^{M_B}\sum_{l=1}^{N_W} W_{i,m,l}^K \Delta\phi_{m,l}^K(n) - \sum_{m=1}^{M_B}\sum_{l=2}^{N_W} W_{i,m,l}^K \Delta\phi_{m,l}(n).\end{aligned}$$

Here, N_B is the number of blades, M_B is the number of panels in the radial direction on the blade, N_W is the number of panels in the streamwise direction of the blade, and N_P is the total number of panels on blade and hub.

The velocities on the boundary surfaces are obtained by differentiating the resulting velocity potential. Once the velocities are found, the pressure distribution is calculated from Bernoulli's equation. Since the coordinate system is fixed on the propeller in this research, the pressure on the propeller blade P_B is obtained by the following equation.

$$P_B = P_\infty - \rho\vec{V}\cdot\nabla\phi - \frac{1}{2}\rho(\nabla\phi)^2, \tag{3}$$

where $\vec{V}$ is the undisturbed inflow velocity vector observed in the moving coordinate system fixed to the propeller axis.

Next, cavitating underwater propeller subjected to a non-uniform inflow is considered. The perturbation potential, $\phi_p(t)$, at any time t and any point p on the wetted surface ($S_{WS}(t)$) or the cavity surface ($S_C(t)$) may be expressed using Green's third identity [4].

$$2\pi\phi_p(t) = \int_{S_{\mathrm{WS}}(t)\cup S_{\mathrm{C}}(t)} \left[\phi_q(t)\frac{\partial}{\partial n_q(t)}\left(\frac{1}{R(p;q)}\right) - \frac{\partial\phi_q}{\partial n_q}(t)\frac{1}{R(p;q)}\right] \mathrm{d}S + \int_{S_{\mathrm{W}}(t)} \Delta\phi_{\mathrm{W}}(t)\frac{\partial}{\partial n_q(t)}\left(\frac{1}{R(p;q)}\right)\mathrm{d}S, \tag{4}$$

where q corresponds to the variable point in the integrations and the unit normal vector $n_q(t)$ corresponds to the wetted surface of the propeller blade, the cavity surface and the trailing wake surface ($S_W(t)$) points into the fluid. $R(p;q)$ is the distance from the point q to the point p and $\Delta\phi_w(t)$ is the potential jump across the trailing wake surface. To determine the unique potential flow solution, the boundary conditions have to be applied on the flow boundaries. However, since the geometry of the cavity surface is unknown, the cavity surface on the blade and wake has to be approximated. Depending on the location of the field point, Eq. (4) can be rewritten and each case may be considered separately. To solve Eq. (4), the propeller blade is discretized into hyperboloidal panels. The time domain is also discretized into equal time intervals. At first, the unsteady non-cavitating problem is solved. And then, the stepwise solution algorithm is applied and the perturbation potentials are obtained at every time step [14]. These values will be used for the calculation of the right-hand side of Eq. (4). Finally, to find the correct cavity planform, Eq. (5) is solved for a given cavitation number.

$$\delta_m(l_1, l_2, \ldots, l_M) = 0, \quad m = 1, \ldots, M, \tag{5}$$

where δ_m is the cavity height at the cavity trailing edge of the mth spanwise strip which is non-dimensionalized by a local chord length and l_m is the cavity length at the same strip. The cavity height can be determined by the kinematic boundary condition. An iterative procedure is required to solve Eq. (5) due to its nonlinear characteristics. From the iterative procedure, the boundary conditions are satisfied on the assumed cavity surface. At every time step, the cavity planform is considered to converge when the maximum of the absolute value of δ is less than 0.001. Details of the method are described in Ref. [4].

2.2. Acoustic prediction

Noise prediction can be represented as the solution of the wave equation if the distribution of sources on the moving boundary (the blade surface) and in the flow field is known. Ffowcs Williams and Hawkings formulated the following equation for the manifestation of acoustic analogy proposed by Lighthill [15]:

$$\frac{1}{c_0^2}\frac{\partial^2 p'}{\partial t^2} - \nabla^2 p' = \frac{\partial}{\partial t}[\rho_0 v_n|\nabla f|\delta(f)] - \frac{\partial}{\partial x_i}[l_i|\nabla f|\delta(f)] - \frac{\partial^2}{\partial x_i\,\partial x_j}[T_{ij}H(f)]. \tag{6}$$

The three source terms on the right-hand side of Eq. (6) are the monopole, dipole and quadrupole terms.

There are various ways to evaluate the Ffowcs Williams–Hawkings equation. Farassat proposed time domain formulation that can predict arbitrary shaped object in motion without the numerical differentiation of the observer time [6,7,16], Farassat Formulation 1A. The Formulation 1A of Farassat is very convenient in embodying the time domain analysis of Ffowcs Williams–Hawkings equation. The quadrupole source term is neglected in this study since the speed of sound in water is much faster than blade rotating speed. The quadrupole term becomes important only for strongly transonic flow.

The field pressure is given as follows [6,16]:

$$p'(\vec{x},t) = p'_T(\vec{x},t) + p'_L(\vec{x},t), \tag{7}$$

where

$$4\pi p'_T(\vec{x},t) = \int_{f=0} \left[\frac{\rho_0 \dot{v}_n}{r(1-M_r)^2}\right]_{\text{ret}} \mathrm{d}S + \int_{f=0} \left[\frac{\rho_0 v_n (r\dot{M}_i \hat{r}_i + c_0 M_r - c_0 M^2)}{r^2(1-M_r)^3}\right]_{\text{ret}} \mathrm{d}S$$

and

$$4\pi p'_L(\vec{x},t) = \frac{1}{c_0}\int_{f=0} \left[\frac{\dot{l}_i \hat{r}_i}{r(1-M_r)^2}\right]_{\text{ret}} \mathrm{d}S + \int_{f=0} \left[\frac{l_r - l_i M_i}{r^2(1-M_r)^2}\right]_{\text{ret}} \mathrm{d}S + \frac{1}{c_0}\int_{f=0} \left[\frac{l_r\left(r\dot{M}_i \hat{r}_i + c_0 M_r - c_0 M^2\right)}{r^2(1-M_r)^3}\right]_{\text{ret}} \mathrm{d}S.$$

Here p'_T and p'_L, respectively, denote the acoustic pressure due to thickness and loading, corresponding to the monopole and the dipole terms. Blade thickness rotation and unsteady sheet cavity volume fluctuation are modeled as monopole sources and blade surface pressure fluctuation is modeled as a dipole source term.

A numerical tool has been developed in this study based on the Formulation 1A of Farassat. As illustrated in Fig. 2, noise prediction starts out from generating a number of discrete panels on the

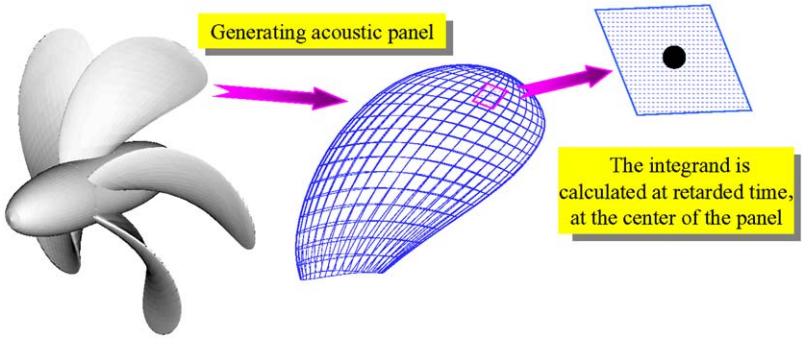

Fig. 2. Procedure of noise prediction.

surface of the blade. Since the integrands in Eq. (7) are then calculated about the mid-point of each panel, the evaluated value is then multiplied by the area of the panel assuming constant strength over the panel. The contributions from all the panels are then added. The addition procedure must be done considering the retarded time equation. The implementation of this formulation is quite straightforward because contributions from each panel and cavity with different retarded times are added to form an acoustic wave. In the subsonic case, the retarded time is calculated by Newton type iteration method. The acoustic pressure history in the observer's time is then formed. The time history of the acoustic pressure is transformed into the noise spectrum in the frequency domain through Fourier transformation.

3. Results and discussion

Basic flow fields of propeller are obtained using a potential-based panel method. In this section, both the flow field and the noise prediction results are presented for non-cavitating/cavitating propeller. The acoustic time history, noise spectra and noise directivity patterns of each noise source are analyzed.

The density and speed of sound in the undisturbed medium, standard water, are 1026 kg/m^3 and 1500 m/s, respectively. The reference pressure for calculating sound pressure level (SPL) is 1.0×10^{-6} Pa. The observer positions are given in terms of the angle θ and the distance d. The observer is located at the distance 10 times the propeller radius, R in the direction of $\theta = 0^\circ$ and $\theta = 90^\circ$ from the propeller shaft axis. The axial angle θ is measured from the downstream propeller axis and the distance d is given in terms of the radius of the propeller, R.

The model propeller having three blades (DTMB4119) is shown in Fig. 3. The propeller was designed by Denny. This model propeller has been distributed to a large number of research institutes through the ITTC Propulsor Committee. The propeller is assumed to be operated at 120 rpm with forward velocity of 1.6 m/s. Flow fields are computed using this propeller model in

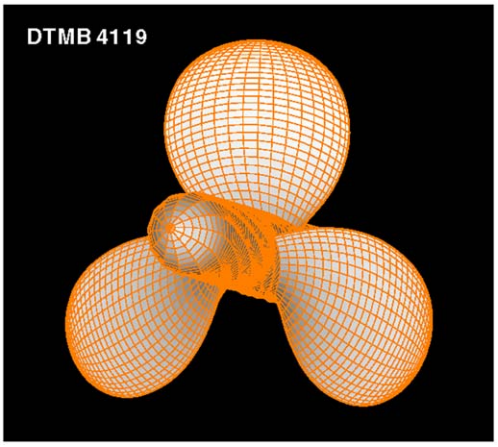

Fig. 3. Single propeller model and condition. DTMB4119 with three blades, rev: 120 rpm, forward speed: 1.6 m/s.

non-uniform flow. Each propeller blade is modeled with 40 spanwise divisions and 80 chordwise divisions (40 for upper surface and 40 for lower surface) to fully consider the thickness of the blade.

3.1. Underwater propeller analysis under non-cavitating condition

In order to validate the unsteady panel method, the results are compared with other numerical methods [11]. The comparison results are shown in Fig. 4, which shows an excellent agreement between the two methods.

Experimentally simulated three-cyclic wake is applied to onset non-uniform inflow. Fig. 5 shows the thrust coefficient comparison of the present method with other numerical methods and experiment. The blade surface pressure contours are shown in Fig. 6.

The noise calculations are performed in various observer positions. The directivity of noise can also be analyzed by this method. The acoustic pressure time history and noise spectra calculated at various positions are shown in Fig. 7. The directivity of the thickness noise is a simple 8-shaped curve with the maximum occurring on the propeller rotation plane. Monopole thickness noise, with its acoustic energy concentrated at its lower harmonics, is known to radiate strongest toward the plane of blade rotation. The unsteady loading noise is known to be dipole in nature, with a strong radiation tendency toward the observer on the hub axis. The results are depicted well in Fig. 8, with the directivity of each noise source computed at the distance of 10R. The unsteady loading noise is mainly governed by irregularities—the fluctuation of surface pressure, while the thickness noise is dominated by the periodicity of propeller rotation. Since the noise prediction is highly affected by inflow conditions, the directivity of the noise generated by propeller in non-uniform flow is complex. Three-dimensional directivity contours are thus shown in Fig. 9. The results show that the overall noise level is highest at the location of the hub center. The trend is the

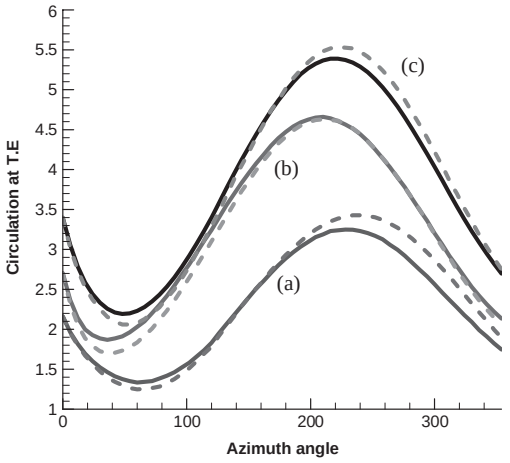

Fig. 4. Comparison with other numerical methods (circulation at trailing edge). (a) $r/R = 0.2940$; (b) $r/R = 0.5960$; (c) $r/R = 0.8278$. Key: —— , present method; - - -, Hsin's method.

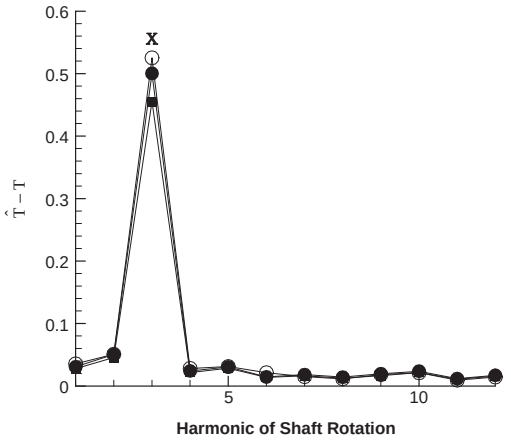

Fig. 5. Thrust coefficient comparison with other numerical methods and experiments. Key: ■, experiment; ○, without viscosity (present method); ●, with viscosity (present method); **X**, Hsin's method.

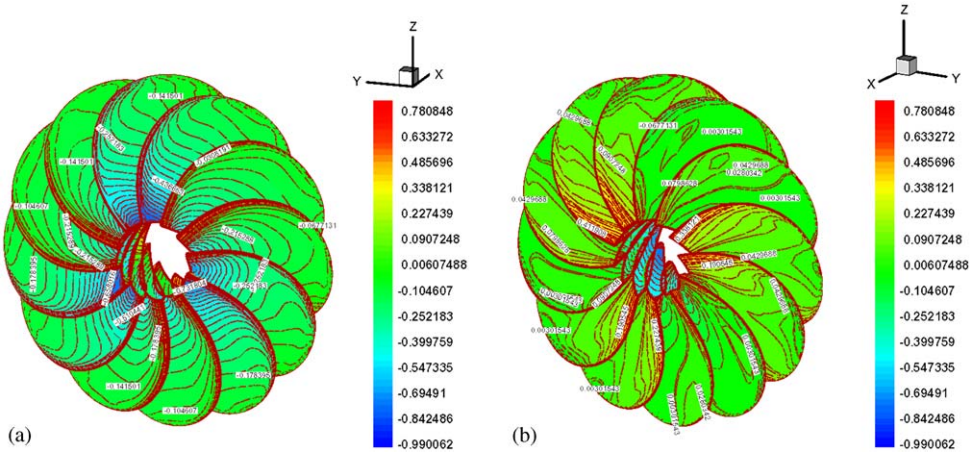

Fig. 6. Blade surface C_p variation of non-cavitating propeller: (a) view from stem (suction side); and (b) view from stern (pressure side).

characteristic of unsteady loading noise, and the monopole noise due to blade thickness is very small compared with the dipole noise.

3.2. *Underwater propeller analysis under cavitating condition*

Finally in order to validate the numerical method for cavitating flow analysis method in non-uniform inflow, it is applied to a modified DTMB 4381 propeller with one blade. The inflow has 15% dent in axial direction and is symmetric about $\theta = 0^\circ$. Fig. 10 shows the cavity volume variation with revolutions. The cavity volume variation from the present method is compared to other numerical results [4,17], and shows a good agreement.

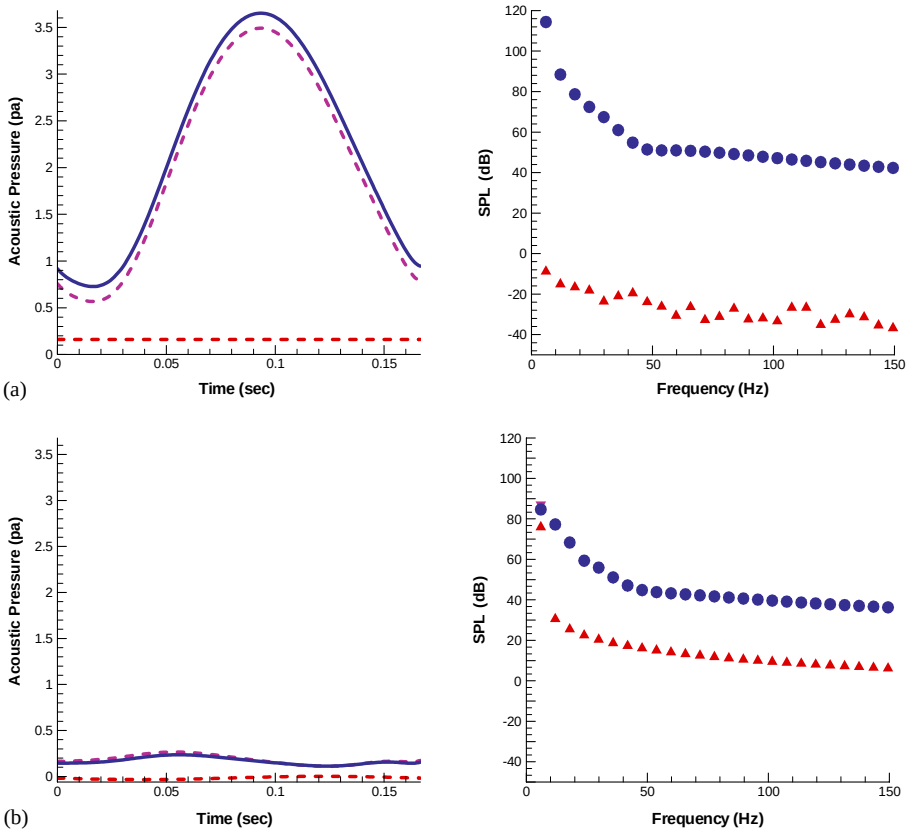

Fig. 7. Acoustic pressure time histories and noise spectra of non-cavitating propeller: (a) $\theta = 0^\circ$, $d = 10$R; (b) $\theta = 90^\circ$, $d = 10$R. Key: - - -, thickness noise; — · — · , loading noise; ——, overall noise: ▲, thickness noise; ▼, loading noise; ●, overall noise.

The propeller model and operating conditions are the same as with the non-cavitating condition, and the cavitation number is fixed at 1.7. Underwater propeller cavitating flow analysis results are shown in Figs. 11 and 12, which displays blade surface pressure distribution and converged sheet cavity planform. These results are then used for noise prediction. As shown in Fig. 11, suction surface pressure distribution is changed due to the cavitation (see Figs. 6(a) and 11(a)). Cavity variations are highly affected by inflow wake. This fact is depicted well in Fig. 12, which shows sheet cavitation shape variation with the azimuth angle. As mentioned earlier, the three cyclic wake is used for the onset of the non-uniform inflow. So sheet cavitation occurs more in the disturbed wake region by inflow condition.

Fig. 13 shows the sheet cavitation SPL (sound pressure level) and directivity. Generally, cavitation noise radiates sound as a monopole but our result shows somewhat weak dipole characteristics. This can be explained by the fact that the sheet cavity is treated as a single volume of vapor attached to the blade surface in this study. Therefore, the blade rotating effect may affect noise directivity.

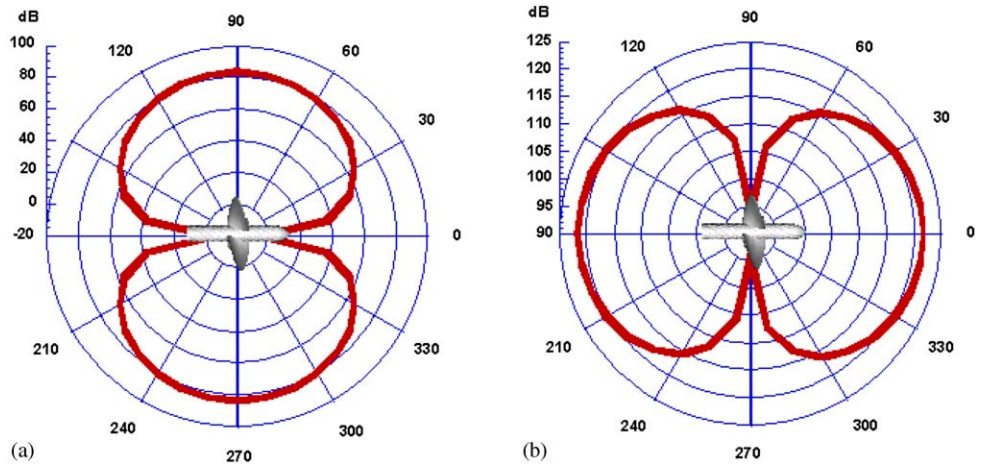

Fig. 8. Each noise directivity of non-cavitating propeller at distance 10R: (a) thickness noise directivity; and (b) loading noise directivity.

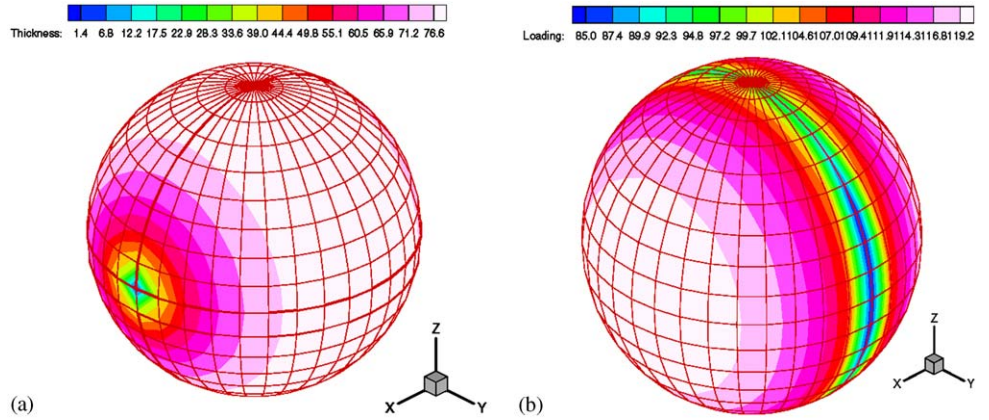

Fig. 9. Thickness and loading noise directivity 3D contour of non-cavitating propeller: (a) thickness noise; and (b) loading noise.

Loading noise characteristics are compared with each other in non-cavitating and cavitating conditions in Fig. 14. As shown in the result, in a non-cavitating condition loading noise is larger than that of cavitating condition. The reason is that the pressure variation in the cavitating region is less than that in the non-cavitating condition. When the sheet cavity covers the part of the blade surface, the cavity-covered surface pressure is equal to the vapor pressure and thus the suction surface pressure variation is limited. Fig. 15 shows the C_p variation at the blade tip where cavitation has occurred. Blade surface C_p variation is larger in the non-cavitation condition. As sheet cavitation develops, vapor cavity covers the parts of the blade surface and thus limits the pressure variation and their performance. But overall

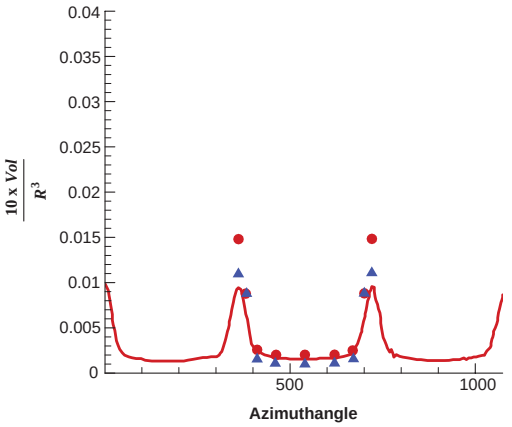

Fig. 10. Cavity volume histories on the DTMB 4381 at $J_s = 0.8$, $\sigma = 2.7$. Key: ——, present method; ●, N. Fine; ▲, C.S. Lee.

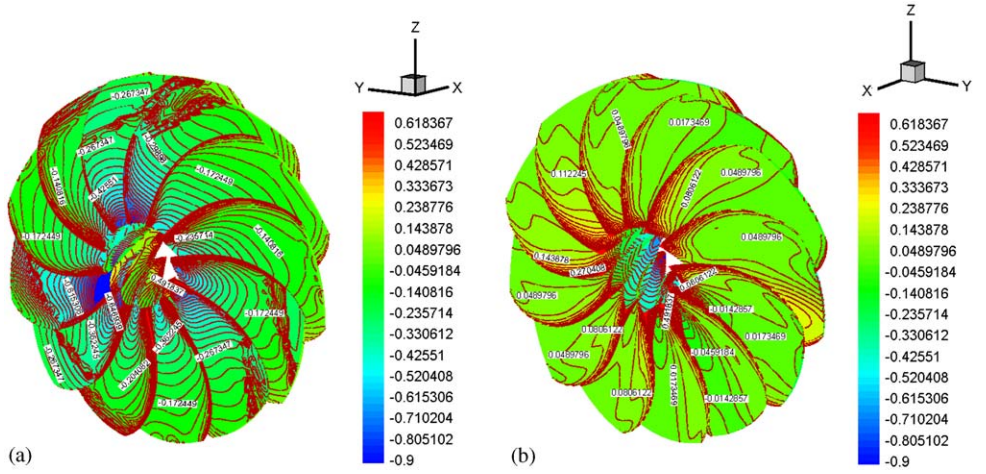

Fig. 11. Blade surface C_p variation of cavitating propeller: (a) view from stem (C_p contour of suction side); and (b) view from stern (C_p contour of pressure side).

noise level under cavitating condition is higher than that of non-cavitation condition. The result is depicted well in Fig. 16, which shows comparison with overall noise level in cavitating and non-cavitating conditions.

4. Conclusion

The non-cavitating and blade sheet cavitation noise generated by an underwater propeller is analyzed numerically in this study. Potential-based panel method coupled with time-domain

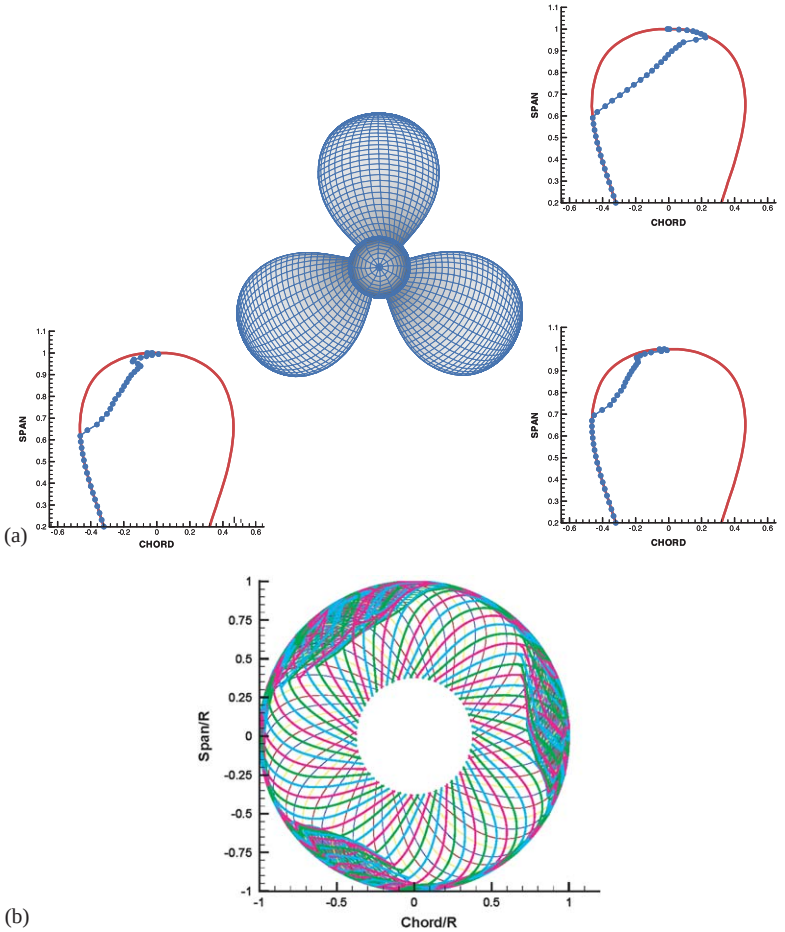

Fig. 12. Shape variation of sheet cavity with the azimuth angle. (a) Shape of sheet cavitation. (b) Shape variation of sheet cavitation.

acoustic analogy is applied to predict the noise generated by underwater propeller in non-uniform flow condition.

The time-stepping potential-based flow solver is modified to increase the time resolution of the flow analysis and the results are compared with other numerical scheme and experiments. The flow solver is proven to be robust and accurate. For noise prediction, Ffowcs Williams–Hawkings equation is adopted in the form proposed by Farassat.

The developed flow solver is applied to the model propeller in uniform and non-uniform inflow. Computed results are shown to be in good agreement with other numerical results and published experimental measurements.

In a non-uniform flow condition similar to the real situation, the noise directivity pattern is a direct result of dipole dominating the overall noise level under non-cavitating condition. But once sheet cavitation occurs, cavitation can be a dominant noise source and loading noise is decreased due to diminution of blade surface pressure variation, caused by sheet cavitation.

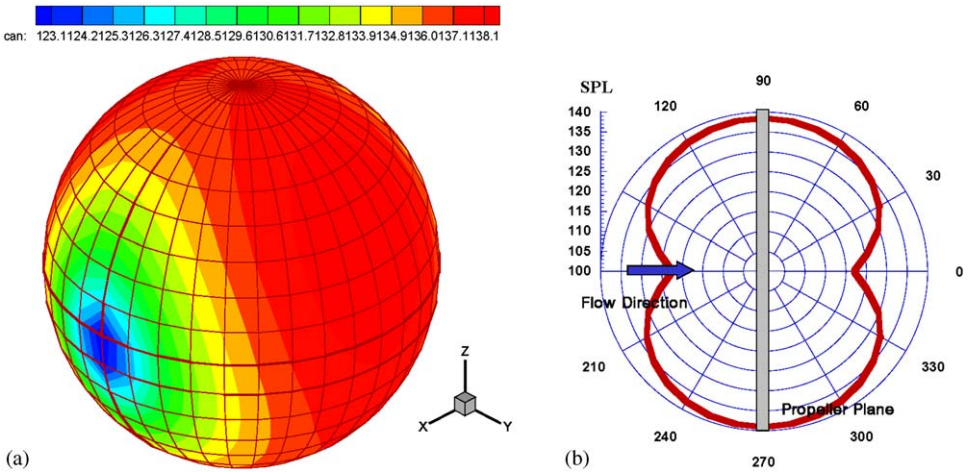

Fig. 13. Sheet cavitation noise 3D contour and directivity: (a) sheet cavitation noise SPL 3D contour; and (b) sheet cavitation noise directivity.

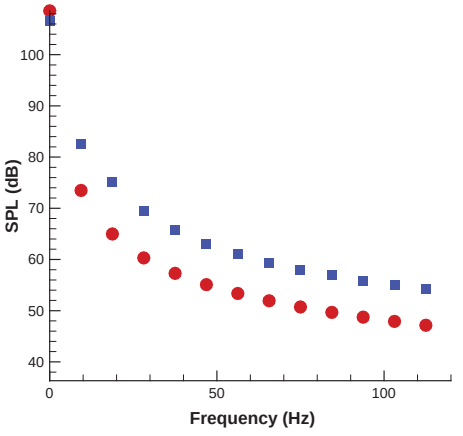

Fig. 14. Comparison of loading noise (cavitating and non-cavitating condition). At $\theta = 0^\circ$, $d = 10R$. Key: ■, non-cavitating condition; ●, cavitating condition.

High frequency noise is excluded in this study because it is too complex to model the real cavity collapse and shock wave dominated by non-linearity. In the field of cavitation study, presently numerical technology is still too poor to describe to that kind of non-linearity and complexity. Therefore some additional problems are remained to solve. High frequency noise of sheet cavitation may be predicted if formation and splitting of bubbles modeling are developed. To solve these problems, more study is needed to clarify the generation mechanism of sheet cavitation break-off and formation to tip vortex cavitation. Although it is exactly predicted from

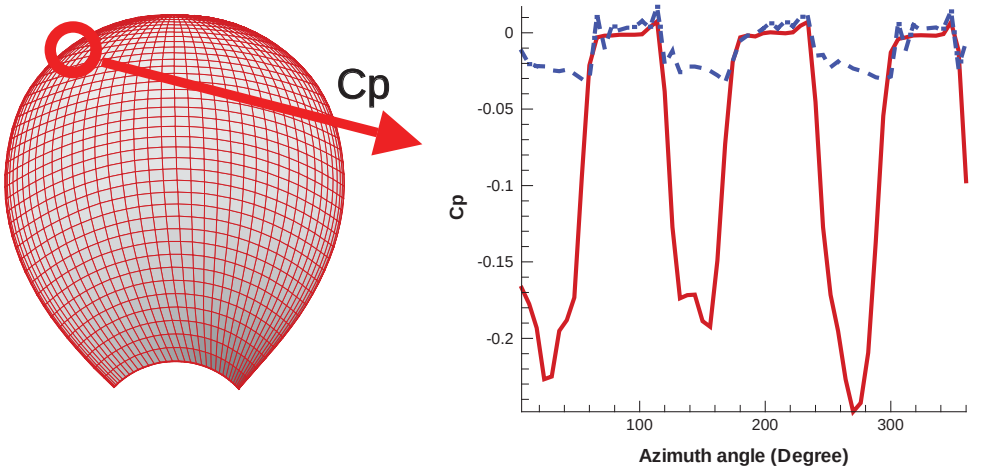

Fig. 15. Comparison of C_p variation according to azimuth angle (non-cavitating and cavitating conditions). Key: ——, non-cavitating condition; - - -, cavitating condition.

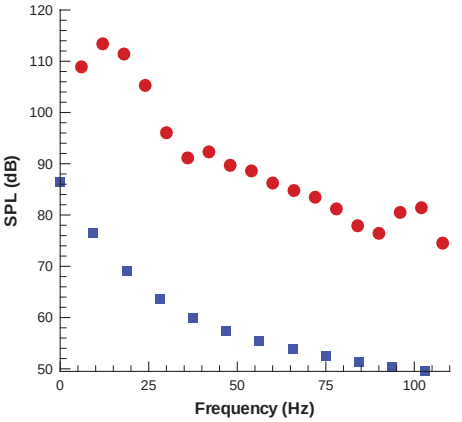

Fig. 16. Comparison of overall noise (cavitating and non-cavitating condition). Key: ■, non-cavitating condition; ●, cavitating condition.

fundamentals, cavitation noise generally rarely follows the experimental results. But numerical analysis based on theory provides a basis for cavitation study and scaling of experimentally measured data.

Acknowledgments

This study was supported by the Underwater Acoustics Research Center (UARC) and the Basic Research Program of KORDI/KRISO. The authors are grateful to Dr. Sangwoo Pyo for his suggestions for the present research.

References

[1] D. Ross, *Mechanics of Underwater Noise*, Pergamon Press, Oxford, 1976.
[2] R.D. Collier, Ship and platform noise, propeller noise, in: M.J. Crocker (Ed.), *Encyclopedia of Acoustics*, Wiley, New York, 1997.
[3] G. Kuiper, New developments around sheet and tip vortex cavitation on ship's propellers, CAV2001, 2001.
[4] N.E. Fine, Nonlinear analysis of cavitating propellers in nonuniform inflow, MIT, Department of Ocean Engineering Report no. 92-5, 1992.
[5] J.E. Ffowcs Williams, D.L. Hawkings, Sound generated by turbulence and surfaces in arbitrary motion, *Philosophical Transactions of the Royal Society A* 264 (1151) (1969) 321–342.
[6] F. Farassat, M.K. Myers, Extensions of Kirchhoff's formula to radiation from moving surfaces, *Journal of Sound and Vibration* 123 (1988) 451–460.
[7] F. Farassat, G.P. Succi, The prediction of helicopter rotor discrete frequency noise, *Vertica* 7 (4) (1983) 309–320.
[8] J.L. Hess, Calculation of potential flow about arbitrary three-dimensional lifting bodied, Technical Report MDC J5679-01, McDonnell Douglas, 1972.
[9] Luigi Morino, Ching-Chiang Kuo, Subsonic potential aerodynamic for complex configurations: a general theory, *AIAA J* 12 (2) (1974) 191–197.
[10] J.E. Kerwin, C.-S. Lee, Prediction of steady and unsteady marine propeller performance by numerical lifting-surface theory, *Transactions of SNAME* (8) (1978).
[11] C.-Y. Hsin, Development and Analysis of Panel Methods for Propellers in Unsteady Flow, PhD Thesis, MIT, Department of Ocean Engineering, 1990.
[12] J.E. Kerwin, S.A. Kinnas, J.-T. Lee, W.-Z. Shin, A Surface panel method for the hydrodynamic analysis of ducted propellers, *Transactions of SNAME* (4) (1987).
[13] S. Pyo, J.-C. Suh, K. Kim, Steady/Unsteady analysis of ducted propellers by using a surface panel method, *Proceedings of the 3rd International Conference on Hydrodynamics*, Seoul, Korea, 1998.
[14] S.A. Kinnas, N.E. Fine, A numerical nonlinear analysis of the flow around two and three dimensional partially cavitating hydrofoils, *Journal of Fluid Mechanics* 254 (1993) 151–181.
[15] M.J. Lighthill, On sound generated aerodynamically, 1. General Theory, *Proceedings of the Royal Society* A211 (1107) (1952) 564–587.
[16] F. Farassat, Theory of noise generation from moving bodies with an application to helicopter rotors, NASA TR R-451, 1975.
[17] C.S. Lee, Prediction of Steady Unsteady Performance of Marine Propellers With or Without Cavitation by Numerical Lifting Surface Theory, PhD Thesis, MIT, Department of Ocean Engineering, 1979.